Microscopic theory of Cooper pair beam splitters based on carbon nanotubes

P. Burset,[1] W. J. Herrera,[2] and A. Levy Yeyati[1]

[1]*Departamento de Física Teórica de la Materia Condensada C-V, Universidad Autónoma de Madrid, E-28049 Madrid, Spain*

[2]*Departamento de Física, Universidad Nacional de Colombia, Bogotá, Colombia*

(Received 8 April 2011; revised manuscript received 24 August 2011; published 26 September 2011)

We analyze microscopically a Cooper pair splitting device in which a central superconducting lead is connected to two weakly coupled normal leads through a carbon nanotube. We determine the splitting efficiency at resonance in terms of geometrical and material parameters, including the effect of spin-orbit scattering. While the efficiency in the linear regime is limited to 50% and decays exponentially as a function of the width of the superconducting region, we show that it can rise to ∼100% in the nonlinear regime for certain regions of the stability diagram.

DOI: 10.1103/PhysRevB.84.115448 PACS number(s): 73.63.Fg, 74.45.+c

I. INTRODUCTION

The production of entangled electron pairs in a solid state device from the splitting of Cooper pairs[1] is a challenging possibility which is starting to generate an intense experimental effort.[2–4] A basic splitting device is a three-terminal system with a central superconducting lead (S) between two normal (N) ones, as depicted in the upper panel of Fig. 1. When a Cooper pair is injected from the S lead it can either be transmitted as a whole to one of the N leads by means of a *local* Andreev reflection process [Fig. 1(a)] or split so that each of the electrons in the pair is transmitted to a different lead, which corresponds to a *crossed* Andreev reflection (CAR) process [Fig. 1(b)].[5] Initial experimental devices were based on nanolithographically defined diffusive samples.[2] In this case a key issue which was extensively addressed theoretically is the competition between CAR processes and direct tunneling of electrons between the normal leads. The cancellation between the two contributions to the nonlocal conductance for thick tunnel barriers was shown to be removed by introducing ferromagnetic leads,[6] increasing the barrier transparency,[7] or taking into account Coulomb interactions.[8] The importance of nonequilibrium effects at large bias voltages has been also analyzed.[9] More recent experiments are oriented toward tunable double-quantum-dot systems based on either carbon nanotubes[3] or InAs nanowires.[4] In spite of the difference in materials the systems realized in both experiments are conceptually equivalent. They did correspond, however, to different physical regimes: while in Ref. 3 the hybridization by direct tunneling between the dots was dominant, in Ref. 4 the direct tunneling appeared to be negligible. In both works the Cooper pair splitting action was demonstrated indirectly by analyzing the changes in the behavior of the conductance when going from the normal to the superconducting state. Both works pointed out an unexpectedly high efficiency for CAR, much higher than would be predicted by theories which do not take into account the direct interdot tunneling.[1] Still further experimental and theoretical efforts are needed in order to demonstrate the splitting unambiguously and to reach the nearly 100% efficiency that might be necessary for entanglement detection.[10]

In the present work we analyze microscopically the case of double quantum dots (DQDs) defined on single-walled carbon nanotubes (SWCNTs) and show that the two regimes of Refs. 3 and 4 can be reached in metallic or semiconducting tubes. We consider the situation illustrated in Figs. 1(c) and 1(d), where the central electrode modifies the electrostatic potential and induces a pairing amplitude on the portion of the tube underneath without breaking its continuity. In agreement with the experimental observations, we show that in this case the splitting efficiency decays rather weakly with increasing width of the central electrode.[4] Our results also suggest how to increase the splitting efficiency up to a level close to 100% by operating the devices in the nonlinear regime. We begin with a SWCNT in the normal state without *e-e* interactions in order to analyze the interdot coupling. Subsequently, we switch on superconductivity in the central electrode and study the probability of CAR processes and the splitting efficiency. Finally, we map the problem onto a minimal model where analytical insight into the nonlinear regime and the effect of interactions is obtained.

II. BASIC MODELING

We focus on zigzag SWCNTs which allow us to consider both metallic and semiconducting cases. If the coupling to the central lead is sufficiently smooth on the atomic scale, we may assume that intervalley scattering is weak and the K-K' degeneracy is preserved. For this case and when the radius is of the order of 1 nm or smaller it is important to consider curvature effects, which produce a finite band gap in metallic tubes and enhance the effect of spin-orbit (SO) interactions. We use two complementary approaches for describing the electronic states in the zigzag SWCNT: a tight-binding (TB) model and a continuous description based on the Bogoliubov–de Gennes–Dirac equations.

Within the continuous description the system is characterized by the equations

$$\begin{pmatrix} H^e_{\tau,s} - E_F & \Delta(x) \\ \Delta(x) & E_F - H^e_{\tau,s} \end{pmatrix} \begin{pmatrix} u_{\tau,s} \\ v_{\tau,s} \end{pmatrix} = E_{\tau,s} \begin{pmatrix} u_{\tau,s} \\ v_{\tau,s} \end{pmatrix}, \qquad (1)$$

where $H^e_{\tau,s} = -i\hbar v_F \partial_x \cdot \sigma_x + \tau \hbar v_F q_n \sigma_y + \tau \delta_0 s - \tau \delta_1 s \sigma_y + V(x)$ is the normal state effective Hamiltonian for the n mode (corresponding to quantized momenta q_n around the tube), $\Delta(x)$ is the induced pairing amplitude, and $V(x)$ is the electrostatic potential profile along the tube. In these equations σ_μ are Pauli matrices in sublattice space, and $\tau, s = \pm$ correspond to the valley and spin indices, respectively. Finally, the terms in δ_0 and δ_1 take into account the SO interaction as

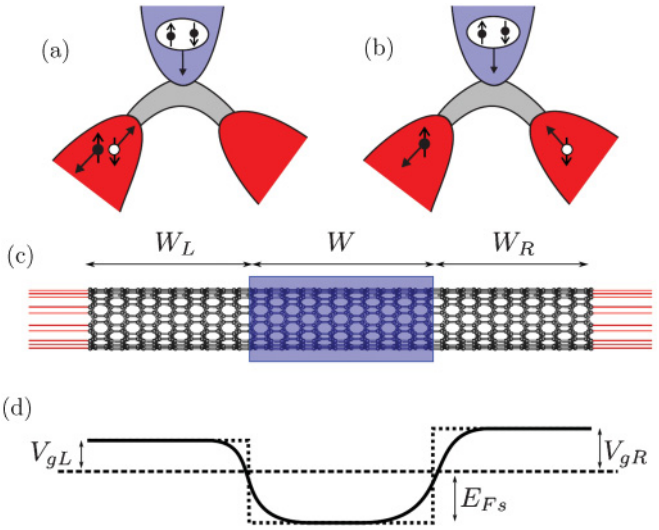

FIG. 1. (Color online) Schematic representation of local (a) and nonlocal (b) Andreev processes in a generic Cooper pair splitter. (c) Specific geometry considered in this work: a finite SWCNT coupled to normal leads at its ends and a central superconducting lead. (d) illustrates the potential profile along the tube.

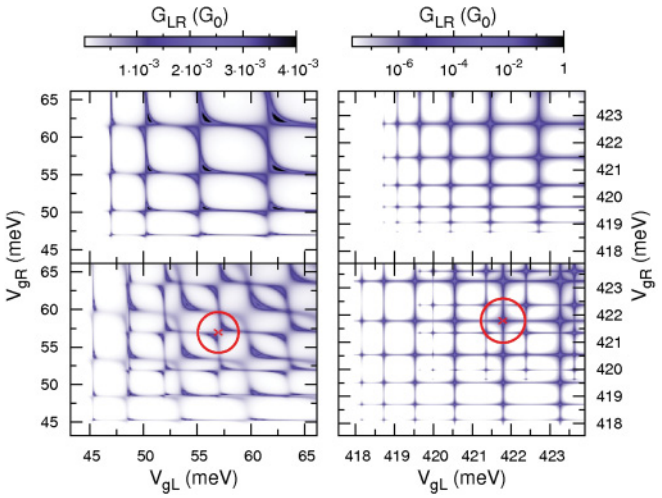

FIG. 2. (Color online) Left panel: Conductance map for a metallic tube ($N = 12$) in the normal state for the p-n-p region with (lower) and without (upper) SO interactions. Right panel: Same for the semiconducting tube ($N = 11$) but in a logarithmic scale. The geometrical parameters are $W = W_{L,R} = 170$ nm.

in Refs. 13. The momenta q_n take the values $\frac{2\pi}{3Na_0}(n \pm \frac{p}{3}) - q_{\rm curv}$, where $p = N \bmod 3 = 0, \pm 1$, a_0 is the interatomic distance and N the number of atoms in the cross section. Depending on whether $p = 0$ or $p = \pm 1$ the tube is metallic or semiconducting, respectively. The curvature effect is included in $q_{\rm curv} = E_{\rm curv}/\hbar v_F$, where $E_{\rm curv} \simeq \pi^2|V_{pp\pi}|/4N^2$ with $|V_{pp\pi}| \simeq 2.7$ eV. In the normal homogeneous case the corresponding energy levels for longitudinal wave vector k are thus given by $E^n_{\tau,s}(k) = \hbar v_F\sqrt{(q_n + \tau s\delta_1)^2 + k^2} + \delta_0\tau s$. The transport properties can be expressed in terms of Green functions which satisfy $[E - \mathcal{H}_{\tau,s}(x)]G_{\tau,s}(x,x') = \delta(x - x')$, where $\mathcal{H}_{\tau,s}(x)$ denotes the full Hamiltonian on the left-hand side of Eq. (1). We obtain these quantities by solving first for the uniform finite regions and then matching the result using the method of Ref. 11.

III. NORMAL STATE

We start by analyzing the linear conductance along the tube, G_{LR}, when the central lead is in the normal state. In Fig. 2 we show a map of G_{LR} in the V_{gL}-V_{gR} plane, obtained using the TB model in the usual nearest-neighbor approximation with a hopping parameter $t \equiv V_{pp\pi}$. As a first approximation the potential profile along the tube is assumed to change discontinuously as represented by the dashed lines in Fig. 1(d). The lateral leads are modeled by ideal one-dimensional (1D) channels weakly coupled to the ends of the tube, as represented schematically in Fig. 1(c). We fix the tunneling rates to these leads to a value $\Gamma_{L,R} \sim 0.01t$, which is consistent with the conductance values observed in Ref. 12 for the lowest-energy states of a SWCNT quantum dot. To model the effect of the central lead we rely on the results of *ab initio* calculations for the case of Al electrodes.[14,15] According to Ref. 14 these produce an n-doping effect, leading to a shift of the tube bands $E_{Fs} \sim -0.5$ eV for an ideal interface. On the other hand, in the normal state it would induce a broadening of the tube levels of the order of a few meV,[15] which suggests a typical value $\Gamma_S \sim 1$ meV for the corresponding tunneling rate. As in the experiments of Ref. 3 the length of the central region is set initially to ~200 nm. We consider tubes with $N = 11, 12$ which correspond to radii $R \sim 0.43, 0.47$ nm, respectively. In the metallic case curvature effects lead to the opening of a narrow gap, which can be estimated as $E_g \simeq E_{\rm curv} \simeq 45$ meV. The curvature gap is apparent in the upper left panel of Fig. 2. On the other hand, in the semiconducting case the gap is $E_g \simeq 412$ meV (top right panel of Fig. 2). It should be noticed that for these diameters and for gate potentials of the order of 0.5 eV only the lowest-energy mode, corresponding to $n = 0$, gives a significant contribution to the transport properties.

For positive V_{gL}, V_{gR}, i.e., in the p-n-p regime, the conductance displays a DQD behavior as shown in Fig. 2. The metallic case (left panels) exhibits an anticrossing pattern similar to the one found in the experiments of Ref. 3. The confinement of the dot states is much more pronounced in the semiconducting case where the Klein tunneling is less significant. We have used a logarithmic scale in this case in order to enhance the visibility of the conductance peaks. When SO scattering is introduced (lower panels in Fig. 2), there is a general splitting of the conductance peaks of the order of ~2 meV due to the breaking of the spin-valley degeneracy. Close to the gap edges this splitting is of the same order as the mean level separation.

IV. SUPERCONDUCTING STATE

When superconductivity in the central lead is switched on, pairing correlations within the tube are induced by proximity effect. The size of the induced gap Δ_i is set by Γ_S. We shall assume that the temperature is zero and that the energy E of the injected electrons from the normal leads is smaller than Δ_i. Then $R_{AL}(E)$ and $R_{AR}(E)$ denote the local Andreev reflection probabilities at the L and R leads, while $T_{\rm CAR}(E)$ corresponds to the CAR processes.

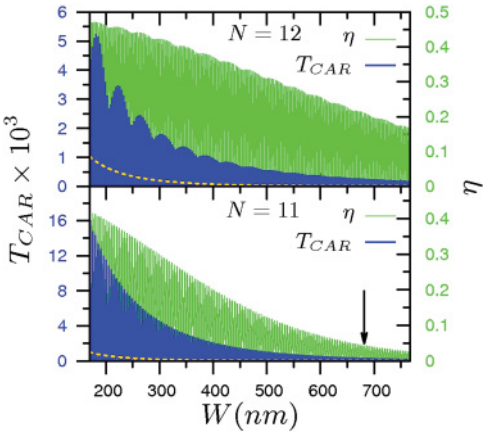

FIG. 3. (Color online) Evolution of the CAR probability (blue or dark gray) and the splitting efficiency η (green or light gray) in the linear regime as a function of the length W of the central electrode for a metallic SWCNT with $N = 12$ (upper panel) and a semiconducting one with $N = 11$ (lower panel). The gate potentials $V_{gL,gR}$ are fixed at the points indicated by the circles in Fig. 2. The dashed lines represent the decay of the CAR probability for a 3D bulk superconductor multiplied by a factor 10^3.

When the system is operated as a beam splitter, a finite voltage difference V is applied between the S and the N leads and the nonlinear conductance is given by $G_{L(R)}(V) = G_0[T_{\rm CAR}(V) + T_{\rm CAR}(-V) + 2R_{AL(R)}(V)]$, with $G_0 = 2e^2/h$ [notice that at finite energy in general $T_{\rm CAR}(E) \neq T_{\rm CAR}(-E)$ due to the breaking of the electron-hole symmetry]. Thus we can define the splitting efficiency as $\eta = G_0[T_{\rm CAR}(V) + T_{\rm CAR}(-V)/(G_L(V) + G_R(V)]$.

Within our model the CAR coefficients decay exponentially on the scale $\xi_0 = \hbar v_F/\Delta_i\sqrt{1-(\hbar v_f q/E_{Fs})^2}$, where $q = q_0 \pm \delta_1/\hbar v_F$, exhibiting oscillations on the scale $\lambda_F = \hbar v_F/|E_{Fs}|$, as illustrated for the linear regime in Fig. 3. In these plots we have fixed the gate voltages at the values indicated by the circles in Fig. 2. The CAR probability decays more slowly in the metallic case ($N = 12$) due to the longer effective coherence length of this case. In both cases, however, the decay is remarkably slower than in a 3D bulk BCS superconductor, where the prediction is $\sim \exp(-2W/\xi_0)/(k_F W)^{2}$,[6] indicated by the dashed lines in Fig. 3. This is a consequence of the single-channel character of the connection between the dots in the present system and explains the rather large efficiency values estimated in recent experiments.[4] As can be observed the efficiency η decreases from 0.4 at $W \sim 200$ nm to <0.05 at $W \sim 700$ nm in the semiconducting case, while it varies between 0.5 and 0.2 for the metallic tube within the same W range. For large W the overall evolution of η is well described by the expression $\eta \sim 1/(1 + \exp 2W/\xi_0)$. This qualitative behavior is also found for a smoother potential profile (see Appendix A).

V. MAP ONTO A MINIMAL MODEL

Further analytical insight is provided by mapping the system onto a minimal model, valid around the crossing points between dot resonances, in which we keep just one twofold-degenerate electron level $E_{L,R}$ in each dot.[16] In the combined dot-Nambu space the model properties can be expressed in terms of bispinor fields $\Psi_\mu = (d_{\mu\uparrow}, d^\dagger_{\mu\downarrow})^T$ where $\mu = L, R$ and $d^\dagger_{\mu\sigma}$ creates dot electrons. In the absence of interactions this reduced model is characterized by a retarded Green function matrix of the form $\hat{G}^{(0)} = [E - \hat{h}_0 + i\hat{\Gamma} - \hat{\Sigma}(E)]^{-1}$, where $(\hat{h}_0)_{\mu\nu,\alpha\beta} = E_\mu \delta_{\mu\nu}\delta_{\alpha\beta}(-1)^{\alpha+1}$, $\mu, \nu \equiv L, R$, $\alpha, \beta \equiv 1,2$ are the Nambu indices, $(\hat{\Gamma})_{\mu\nu,\alpha\beta} = \tilde{\Gamma}_\mu \delta_{\mu\nu}\delta_{\alpha\beta}$ with $\tilde{\Gamma}_\mu = \Gamma_\mu a_0/W_\mu$ correspond to the effective tunneling rates to the normal leads, and $\hat{\Sigma}$ is a matrix self-energy describing the coupling with the central superconducting region (see Appendix B). Of particular importance for determining the splitting performance of the device is the quantity $\Sigma_{LR,12}$ associated with the interdot CAR processes. In the long-W limit this reduces to

$$\Sigma_{LR,12} \sim \frac{t a_0 e^{-W/\xi(E)}}{2\sqrt{W_L W_R}} \frac{\Delta_i}{\sqrt{E^2 - \Delta_i^2}} \sin(k_0 W + \alpha_s), \qquad (2)$$

where $k_0 = \sqrt{(E_{Fs}/\hbar v_F)^2 - q^2}$, $e^{i\alpha_s} = \hbar v_F(k_0 + iq)/E_{Fs}$, and $\xi(E) = \xi_0 \Delta_i/\sqrt{\Delta_i^2 - E^2}$. To the lowest order in $\hat{\Sigma}$, $T_{\rm CAR}(E) \sim |\Sigma_{LR,12}/[(E - E_L + i\tilde{\Gamma}_L)(E + E_R + i\tilde{\Gamma}_R)]|^2$, which suggests that it would be maximized for $E \sim E_L \sim -E_R$. Further analysis shows that $\eta \to 1$ could be obtained provided that $\Delta_i > |E_L| \gg \tilde{\Gamma}_{L,R} e^{W/\xi(E_L)}$. As we show below, these predictions are confirmed by the full calculations where we additionally include the effect of interactions.

For this purpose we assume a constant charging energy $U_{L,R} \gg \Delta_i$ acting on each dot and apply the equation of motion (EOM) technique with a Hartree-Fock decoupling at the level of the two-body Green functions as described in Appendix C. This approximation is valid when Kondo and exchange correlations between the dots can be neglected. Further simplification is achieved in the limit $U_\mu \to \infty$, where we find $\hat{G} = [\hat{g}^{-1} + i\hat{\Gamma} - \hat{\Sigma}]^{-1}$, with $g = (E - \hat{h}_0)^{-1}[1 - \hat{A}_\infty]$ and $(\hat{A}_\infty)_{\mu\nu,\alpha\beta} = n_\mu \delta_{\mu\nu}\delta_{\alpha\beta}$. The evaluation of the mean values $n_\mu = \langle d^\dagger_{\mu\sigma} d_{\mu\sigma}\rangle$ must be performed self-consistently.

The main effect of interactions within this approximation is to shift the resonances and to reduce their width, roughly as $(1 - n_\mu)\tilde{\Gamma}_\mu$. Then, the CAR and the local Andreev probabilities are reduced by factors $(1 - n_1)(1 - n_2)$ and $(1 - n_\mu)^2$, respectively, which therefore do not modify significantly the efficiency at resonance. The color map in Fig. 4(a) shows the efficiency in the linear regime corresponding to the semiconducting case with $W \sim 700$ nm (arrow in Fig. 3) and for the region of gate voltages indicated by the circle in the right panel of Fig. 2. As can be observed, η exhibits maximum values at the crossing points between resonances of the order of 0.1, slightly higher than the values found in the noninteracting case. The efficiency reaches a maximum of the same magnitude along the line $E_L \sim -E_R$ (red dashed line).

A. Nonlinear regime

What is more remarkable is that the efficiency along this line rises to ~100% in the nonlinear regime $V \neq 0$. This is illustrated in Fig. 4(b). The high-efficiency regions lie within the dot resonances (indicated by the dashed white lines) which are shifted from zero energy due to the presence of an induced

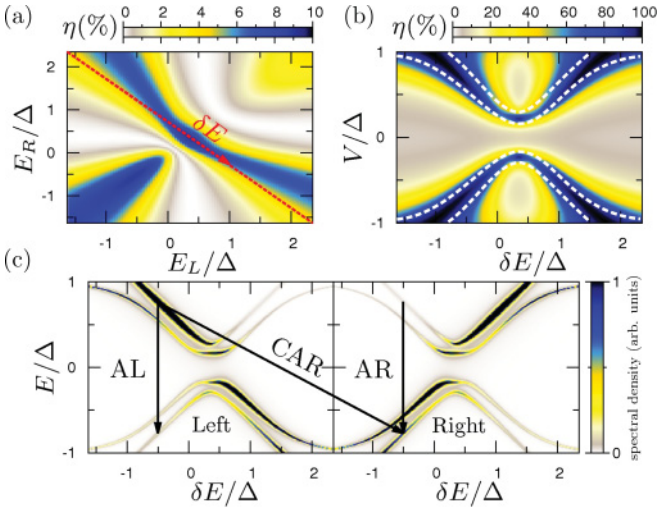

FIG. 4. (Color online) Color map of the splitting efficiency within the minimal model with parameters corresponding to a semiconducting tube with $W \sim 700$ nm (indicated by the arrow in Fig. 3) in the linear (a) and nonlinear (b) regimes. In the latter case the dot levels are varied along the line $E_L \sim -E_R$ indicated by the dashed red line of (a). The white dashed lines indicate the maxima in the spectral density, which is shown in (c) for the two dots along this line. Local and nonlocal Andreev processes at finite V are indicated by the black arrows.

minigap and split due to the hybridization between the dots. This last effect is linked to the matrix elements $\Sigma_{LR,\mu\mu}$.

The origin of these high-efficiency regions can be understood qualitatively from the spectral density on each dot, which is shown in Fig. 4(c). As can be observed, the electron-hole symmetry in the local spectral density is lost along the line $E_L \sim -E_R$. Crossed Andreev processes like the one sketched as the CAR arrow in Fig. 4(c) combine electron and hole states on each dot with high spectral density. These interdot transitions are then more favorable than the intradot electron-hole conversions (arrows AR and AL), in which either the electron or the hole state has low spectral density. As a consequence, local Andreev processes become suppressed while nonlocal CAR processes are enhanced, thus explaining the efficiency increase. It should be stressed that this increase is mainly due to an energy filtering mechanism,[17] which is only weakly affected by Coulomb interactions.

VI. CONCLUSIONS

We have analyzed the splitting efficiency of SWCNT double-quantum-dot devices in terms of material and geometrical parameters. The single-channel character of the connection between the dots in this configuration explains the weak decay of CAR with distance, which is consistent with the experimental observations. Furthermore we have shown how the splitting efficiency can rise to ∼100% by working in the nonlinear regime. We expect that our analysis can guide future experiments for the production of entangled electron pairs using these devices. In this respect the appearance of recent experimental results by Hofstetter *et al.*[18] is encouraging; they extend the study of Cooper pair splitters based on semiconducting nanowires to the nonlinear regime.

ACKNOWLEDGMENTS

The authors would like to thank T. Kontos, A. Cottet, and R. Egger for fruitful discussions. This work was supported by MICINN-Spain via Grant No. FIS2008-04209, the EU FP7 project SE^{2}ND (P.B. and A.L.Y.), and DIB from Universidad Nacional de Colombia, Project No. 12170 (W.J.H.).

APPENDIX A: EFFECT OF SMEARING THE POTENTIAL PROFILE

For the results of Figs. 2 and 3 the electrostatic potential profile along the tube has been assumed to change discontinuously at the interfaces with the central region. It is thus defined as

$$V(x) = \begin{cases} V_{gL}, & 0 \leqslant x \leqslant W_L, \\ E_{Fs}, & W_L < x \leqslant W_L + W, \\ V_{gR}, & W_L + W < x \leqslant W_T, \end{cases} \tag{A1}$$

where $W_T = W_L + W + W_R$.

However, a more realistic description would correspond to a smooth potential as defined by

$$V(x) = E_{Fs} + \frac{V_{gL} - E_{Fs}}{\pi}\left[\frac{\pi}{2} - \arctan\frac{x - W_L}{\alpha a_0}\right] + \frac{V_{gR} - E_{Fs}}{\pi}\left[\frac{\pi}{2} + \arctan\frac{x - W_L - W}{\alpha a_0}\right], \tag{A2}$$

where the parameter α controls the smearing of the potential at the interfaces. This smooth electrostatic potential displaces the position of the energy levels of the dots, thus changing the position of the resonance in the V_{gL}-V_{gR} map. Nevertheless, the overall features of the conduction maps are not modified. In Fig. 5 we show the evolution of the splitting efficiency η as a function of the length W of the central electrode for a semiconducting case with $N = 11$ and gate potentials corresponding to the resonance indicated by the centers of the red circles of Fig. 2. Different values of the parameter α are shown along with the case $\alpha \to 0$, which corresponds to the square barrier potential given by Eq. (A1). The main effect of the smeared potential is a change of phase in the oscillatory pattern at the atomic scale. However, in all cases, the efficiency

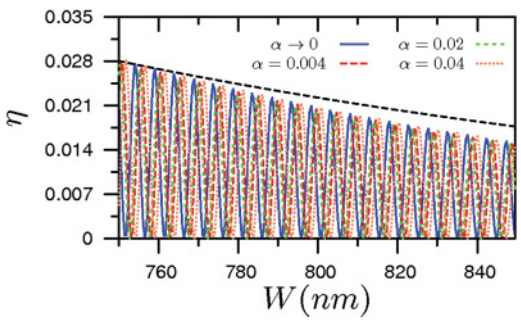

FIG. 5. (Color online) Evolution of the splitting efficiency η as a function of the length W of the central electrode for $N = 11$. Different values of the parameter α are shown, representing different electrostatic potential profiles. The asymptotic behavior $\eta \sim 1/[1 + \exp 2W/\xi(q)]$ is indicated by the black dashed line. The gate potentials $V_{gL,gR}$ are fixed at the values indicated by the centers of the circles of Fig. 2 in the main text.

fits very well the functional form $\eta \sim 1/[1+\exp 2W/\xi(q)]$ indicated by the black dashed line in Fig. 5.

APPENDIX B: SELF-ENERGY DESCRIBING THE COUPLING WITH THE SUPERCONDUCTING ELECTRODE

We provide here some details on the self-energy between the dots and the central superconducting region within the minimal model discussed in the paper. First, we need the propagator for the finite nanotube region of width W in which superconductivity has been induced. Following the method of Ref. 11, this can be written as

$$g_{s,ab} = \left(\frac{F^1_{ab}}{\Omega}(E+\sigma_x\Delta_i)+\sigma_z F^2_{ab}\right),$$

where $\Omega=\sqrt{E^2-\Delta_i^2}$, Δ_i is the induced pairing amplitude, the indices $a,b=L,R$ denote the two edges of this region, σ_x,σ_z are the Pauli matrices in Nambu space, the functions $F^{1,2}_{ab}$ depend on W and are of the form

$$F^{1,2}_{LR}=F^{1,2}_{RL}=\frac{\cos\alpha_-}{2\cos(k_-W+\alpha_-)}\mp\frac{\cos\alpha_+}{2\cos(k_+W+\alpha_+)},$$
$$F^{1,2}_{LL}=F^{1,2}_{RR}=\frac{i\sin k_-W}{2\cos(k_-W+\alpha_-)}\mp\frac{i\sin k_+W}{2\cos(k_+W+\alpha_+)},$$

$k_\pm=\sqrt{(E_F\pm\Omega)^2/\hbar^2v_F^2-q^2}$, and $e^{i\alpha_\pm}=(k_\pm+iq)/\sqrt{k_\pm^2+q_0^2}$. With this, the self-energy between the dots and the superconductor is given by

$$\Sigma_{ab}=\sqrt{\tilde\Gamma_a\tilde\Gamma_b}\sigma_z g_{s,ab}\sigma_z,$$

where $\tilde\Gamma_a$ are the effective tunneling rates from the central region to the dots, $\tilde\Gamma_a=ta_0|\sin(k_{0a}W_a)\cos\alpha_a|/(2W_a)$, k_{0a} being the wave vector for the corresponding dot state and $\cos\alpha_a=k_{0a}/\sqrt{k_{0a}+q^2}$.

APPENDIX C: EQUATION OF MOTION APPROACH TO INCLUDE INTERACTIONS

In this section we describe the approximation used to include interactions within the minimal model for the S DQD system. The dot levels will be indicated by the indices $\mu=L,R$ (dot) and $\sigma=\uparrow,\downarrow$ (spin). The Hamiltonian of the system is

$$\hat H=\hat H_L+\hat H_R+\hat H_S+\hat H_T+\hat H_{DS}+\sum_{\mu,\sigma}E_\mu\hat n_{\mu\sigma}+\sum_\mu U_\mu\hat n_\mu(\hat n_\mu-1)/2, \quad \text{(C1)}$$

where $d^\dagger_{\mu\sigma}$ creates an electron in dot μ with spin σ, $\hat n_{\mu\sigma}=\hat d^\dagger_{\mu\sigma}d_{\mu\sigma}$, $\hat n_\mu=\sum_\sigma\hat n_{\mu\sigma}$, and $\hat H_{L,R,S}$ describe the isolated left, right, and central superconducting leads, respectively. Finally $\hat H_T$ corresponds to the tunnel coupling between the dot level and the normal leads while H_{DS} couple the dots to the superconducting electrode.

The transport properties of this model can be adequately described in terms of the DQD retarded Green functions in Nambu space, defined as $\hat G(\tau)=-i\theta(\tau)\langle[\hat\psi(\tau),\hat\psi^\dagger(0)]_+\rangle$, where $\hat\psi_\mu=(d_{\mu,\uparrow},d^\dagger_{\mu,\downarrow},d_{\mu,\uparrow},d^\dagger_{\mu,\downarrow})$ is a bispinor in Nambu space. To simplify the notation we shall use hereafter $\hat G=\langle\langle\hat\psi;\hat\psi^\dagger\rangle\rangle$. To deal with the interaction we rely here on an equation of motion approach, with a decoupling at the level of the two-particle Green functions. From the equation of motion for $\hat G$, in frequency representation we obtain

$$[\omega\hat I-\hat h_0+i\hat\Gamma-\hat\Sigma]\hat G=\hat I+\hat U\hat W, \quad \text{(C2)}$$

where $(\hat h_0)_{\mu\nu,\alpha\beta}=\delta_{\mu\nu}\delta_{\alpha,\beta}(-1)^{\alpha+1}E_\mu$, $(\hat U)_{\mu\nu,\alpha\beta}=\delta_{\mu\nu}\delta_{\alpha\beta}(-1)^{\alpha+1}U_\mu$, and $\hat W=\langle\langle\ \hat\phi;\hat\psi^\dagger\rangle\rangle$, with $(\hat\phi)_{\mu,\alpha}=\delta_{\alpha,1}d_{\mu\uparrow}n_{\mu\downarrow}+\delta_{\alpha,2}d^\dagger_{\mu\downarrow}n_{\mu\uparrow}$. $\hat W$ is a two-body Green function generated by the presence of the U terms in the model Hamiltonian. The tunneling rates $(\hat\Gamma)_{\mu\nu,\alpha\beta}=\Gamma_\mu a_0/W_\mu\delta_{\mu\nu}\delta_{\alpha\beta}$ arise from the coupling to the normal leads, while $\hat\Sigma$ is the matrix self-energy described in the previous section. To close the system of equations we analyze the EOM for $\hat W$ and introduce a mean-field decoupling scheme for the rest of the two-body Green functions which are generated. In this way we obtain

$$(\omega\hat I-\hat h_1)\hat W=\hat A[1+(\hat\Sigma-i\hat\Gamma)\hat G], \quad \text{(C3)}$$

where $(\hat A)_{\mu\nu,\alpha\beta}=\delta_{\mu\nu}(\delta_{\alpha\beta}\langle n_\mu\rangle+(1-\delta_{\alpha\beta})\langle\hat d_{\mu\uparrow}\hat d_{\mu\downarrow}\rangle)$ and $\hat h_1=\hat h_0+\hat U$.

Extracting $\hat W$ from (C3) and substituting in (C2), we obtain an expression for $\hat G$ which can be evaluated self-consistently:

$$\hat G=[\omega-\hat h_0+i\hat\Gamma-\hat\Sigma-\hat U(\omega-\hat h_1)^{-1}\hat A(-i\hat\Gamma+\hat\Sigma)]^{-1}\times[\hat I+\hat U(\omega-\hat h_1)^{-1}\hat A]. \quad \text{(C4)}$$

This can be written in a more compact way as

$$\hat G=[\hat g^{-1}+i\hat\Gamma-\hat\Sigma]^{-1}, \quad \text{(C5)}$$

where

$$\hat g=(\omega-\hat h_0)^{-1}[\hat I+\hat U(\omega-\hat h_1)^{-1}\hat A].$$

Finally, taking the limit $U_\mu\to\infty$, further simplification occurs as one can safely neglect the induced pairing correlations $\langle\hat d_{\mu\uparrow}\hat d_{\mu\downarrow}\rangle$.[19] This allows one to write

$$\hat g\to(\omega-\hat h_0)^{-1}[\hat I-\hat A_\infty], \quad \text{(C6)}$$

where $(\hat A_\infty)_{\mu\nu}=\delta_{\mu\nu}\langle n_\mu\rangle$.

[1] P. Recher, E. V. Sukhorukov, and D. Loss, Phys. Rev. B **63**, 165314 (2001); N. M. Chtchelkatchev, G. Blatter, G. B. Lesovik, and T. Martin, *ibid.* **66**, 161320 (2002); C. Bena, S. Vishveshwara, L. Balents, and M. P. A. Fisher, Phys. Rev. Lett. **89**, 037901 (2002); P. Samuelsson, E. V. Sukhorukov, and M. Büttiker, *ibid.* **91**, 157002 (2003).

[2] D. Beckmann, H. B. Weber, and H. V. Löhneysen, Phys. Rev. Lett. **93**, 197003 (2004); S. Russo, M. Kroug, T. M. Klapwijk, and

A. F. Morpurgo, *ibid*. **95**, 027002 (2005); P. Cadden-Zimansky and V. Chandrasekhar, *ibid.* **97**, 237003 (2006); A. Kleine, A. Baumgartner, J. Trbovic, and C. Schönenberger, Europhys. Lett. **87**, 27011 (2009); J. Wei and V. Chandrasekhar, Nature Phys. **6**, 494 (2010).

[3]L. G. Herrmann, F. Portier, P. Roche, A. Levy Yeyati, T. Kontos, and C. Strunk, Phys. Rev. Lett. **104**, 026801 (2010).

[4]L. Hofstetter, S. Csonka, J. Nygard, and C. Schönenberger, Nature (London) **461**, 960 (2009).

[5]G. Deutscher and D. Feinberg, Appl. Phys. Lett. **76**, 487 (2000).

[6]G. Falci, D. Feinberg, and F. W. J. Hekking, Europhys. Lett. **54**, 255 (2001); R. Mélin and D. Feinberg, Phys. Rev. B **70**, 174509 (2004).

[7]J. P. Morten, A. Brataas, and W. Belzig, Phys. Rev. B **74**, 214510 (2006); M. S. Kalenkov and A. D. Zaikin, *ibid*. **75**, 172503 (2007); R. Mélin, F. S. Bergeret, and A. Levy Yeyati, *ibid.* **79**, 104518 (2009).

[8]A. Levy Yeyati, F. S. Bergeret, A. Martín-Rodero, and T. M. Klapwijk, Nature Phys. **3**, 455 (2007).

[9]F. S. Bergeret and A. Levy Yeyati, Phys. Rev. B **80**, 174508 (2009).

[10]V. Bouchiat, N. Chtchelkatchev, D. Feinberg, G. B. Lesovik, T. Martin, and J. Torrès, Nanotechnology **14**, 77 (2003).

[11]W. J. Herrera, P. Burset, and A. Levy Yeyati, J. Phys.: Condens. Matter **22**, 275304 (2010).

[12]F. Kuemmeth, S. Illani, D. C. Ralph, and P. L. McEuen, Nature (London) **452**, 448 (2008).

[13]J.-S. Jeong and H-W. Lee, Phys. Rev. B **80**, 075409 (2009); S. Weiss, E. I. Rashba, F. Kuemmeth, H. O. H. Churchill, and K. Flensberg, *ibid*. **82**, 165427 (2010).

[14]G. Giovannetti, P. A. Khomyakov, G. Brocks, V. M. Karpan, J. van den Brink, and P. J. Kelly, Phys. Rev. Lett. **101**, 026803 (2008).

[15]S. Barraza-Lopez, M. Vanevic, M. Kindermann, and M. Y. Chou, Phys. Rev. Lett. **104**, 076807 (2010).

[16]The effect of SO interactions is to break the fourfold degeneracy and it is thus implicitly taken into account in the minimal model.

[17]M. Veldhorst and A. Brinkman, Phys. Rev. Lett. **105**, 107002 (2010).

[18]L. Hofstetter, S. Csonka, A. Baumgartner, G. Fülöp, S. d'Hollosy, J. Nygard, and C. Schönenberger, Phys. Rev. Lett. **107**, 136801 (2011).

[19]J. C. Cuevas, A. Levy Yeyati, and A. Martín-Rodero, Phys. Rev. B **63**, 094515 (2001); Y. Tanaka, N. Kawakami, and A. Oguri, J. Phys. Soc. Jpn. **76**, 074701 (2007).